Materials Chemistry and Physics 238 (2019) 121870

Contents lists available at ScienceDirect

Materials Chemistry and Physics

journal homepage: www.elsevier.com/locate/matchemphys

Enhanced lithium/sodium storage of SnO_2/Graphene aerogels nanocomposites

Linlin Fan [a], Dongbin Xiong [a], Xifei Li [a,b,c,*]

[a] Institute of Advanced Electrochemical Energy & School of Materials Science and Engineering, Xi'an University of Technology, Xi'an, 710048, China
[b] Tianjin International Joint Research Centre of Surface Technology for Energy Storage Materials, College of Physics and Materials Science, Tianjin Normal University, Tianjin, 300387, China
[c] State Center for International Cooperation on Designer Low-carbon & Environmental Materials (CDLCEM), Zhengzhou University, 100 Kexue Avenue, Zhengzhou, 450001, China

HIGHLIGHTS

- SnO_2 nanoparticles with 5–8 nm size can decrease diffusion lengths of Li^+/Na^+.
- Graphene aerogel can effectively relieve SnO_2 expansion/shrinkage upon cycling.
- The optimized mass loading of SnO_2 nanoparticles facilitates capacity improvements.

ARTICLE INFO

Keywords:
Lithium ion batteries
Sodium ion batteries
Electrochemical stability
SnO_2 soliquid
Graphene aerogels

ABSTRACT

SnO_2/graphene aerogels (SnO_2/GAs) nanocomposites are fabricated via a cost-efficient hydrothermal and large-scalable strategy. In present study, SnO_2 nanoparticles possessing various contents are loaded onto the surface of GAs to optimize the electrochemical activity of nanocomposite systems as anodes for lithium ion batteries (LIBs) and sodium ion batteries (SIBs). SEM and TEM characterizations obviously show SnO_2 nanoparticles with the diameter of 5–8 nm are dispersed homogeneously on GAs through present synthetic process. Remarkably, the optimized SnO_2/GAs demonstrates excellent cycling performance and stability as a LIB anode while delivering discharge capacity of 935 mAh g^{-1} upon 350 cycles at 100 mA g^{-1}, accounting for 98.8% of the 2nd reversible capacity. Moreover, as for SIB, SnO_2/GAs anode can deliver a discharge capacity of 274 mAh g^{-1} at 50 mA g^{-1} after 100 cycles, which is 91.3% of the reversible capacity in the second cycle. The outstanding electrochemical stability benefits from synergistic effects of SnO_2 nanoparticles as well as GAs matrix offering large surface area. Hence, consideration of superior electrochemical property and high yield, the SnO_2/GAs nanocomposite presents a great potential for the electrochemical energy storage.

1. Introduction

Currently, lithium ion batteries (LIBs) have received widespread attention all over the world as energy storage technology due to their long lifespan, high security, and excellent energy density [1]. In addition to portable devices, they are used in hybrid electric vehicles and electric vehicles and have developed into one of the dominant energy storage devices. However, the lithium reserves are limited and they can't satisfy the increased demands on LIBs. Fortunately, the sodium resources are abundant and unlimited in the Earth crust [2,3]. Meanwhile, sodium exhibits similar chemical properties as well as the similar "rocking-chair" sodium storage mechanism to that of lithium [4]. So sodium ion batteries (SIBs) are another hopeful energy reserve system.

For commercial LIBs, graphite with low theoretical capacity of 372 mAh g^{-1} suffers from limited power and energy performance when employed as anode material [5]. In addition, graphite is inapplicable to SIBs because of large ionic radius of sodium as well as thermodynamically instability of sodium-graphite system [6]. It is highly demanded to develop suitable anode materials with superior capacity, low cost, and high rate of charge for LIBs/SIBs. As a typical transition metal oxide, SnO_2 with excellent theoretical capacity has been considered as a potential anode material [7]. Nevertheless, SnO_2 suffers from dramatic

* Corresponding author. Institute of Advanced Electrochemical Energy & School of Materials Science and Engineering, Xi'an University of Technology, Xi'an, 710048, China.
E-mail address: xfli2011@hotmail.com (X. Li).

https://doi.org/10.1016/j.matchemphys.2019.121870
Received 21 August 2018; Received in revised form 4 July 2019; Accepted 12 July 2019
Available online 13 July 2019
0254-0584/

volume expansion during cycling processes, pulverization and poor circulation characteristic severely restrict its practical applications [8]. Designing various SnO_2 heterostructures and morphologies, such as nanorod array [9], quantum dots [10], hollow nanospheres [11] and so on, is a potential approach to restrain these drawbacks. These SnO_2 could greatly relieve pressure from the contraction or expansion upon the charge-discharge process. Another available strategy is to synthesize nanosized SnO_2 with carbonaceous materials, including SnO_2@carbon core-shell spheres [12], Sn/SnO_2/porous carbon [13], graphene-encapsulated CNT@SnO_2 [14], all of the composites mentioned above ensure the implementation of electrode integrity and display the enhanced electrochemical properties.

Herein, we synthesize SnO_2 soliquid with high stability and reactivity, and a facile hydrothermal method is employed to prepare SnO_2/graphene aerogels (denoted as SnO_2/GAs) nanocomposites. As observed from Scheme 1, the positively charged SnO_2 soliquid can be coupled with negatively charged graphite oxide (GO) by electrostatic interactions. Following a chemical reduction by hydrothermal process, the GO in SnO_2/GO is converted into GAs with forming SnO_2/GAs composites. SnO_2 nanoparticles are distributed on GAs and a systematic study is conducted to explore the effect of different SnO_2 contents in nanocomposites for superior anodes performance of LIBs/SIBs. The optimized SnO_2/GAs nanocomposites exhibit stable electrochemical performance and long lifespan. Moreover, the limitations related to volume expansion are minimized in this case because of GAs with high surface area along with nano-sized SnO_2 particles. We anticipate that this technique may provide significant contributions to the development of anode materials in energy storage systems.

2. Experimental section

2.1. Synthesis of the SnO_2 soliquid

10.2 mL acetylacetone was added to 37.6 mL *n*-butyl alcohol under constant magnetic stirring efficiently. After the formation of homogeneous suspension, 34.2 mL $SnCl_4$ was added into above solution drop by drop at room temperature. The resultant mixed solution was labeled as solution A. Subsequently, solution B was prepared by dissolving 3.804 g *p*-toluenesulfonic acid in 18 mL deionized water. After mixing of the two solutions, the resultant mixture was then transferred to a flask, stirred at 60 °C for 12 h under reflux. Finally, light yellow and transparent SnO_2 soliquid was obtained.

2.2. Synthesis of SnO_2/GAs nanocomposites

GO was prepared via the method reported in our previous work [15, 16]. Typically, fixed amount of SnO_2 soliquid was dispersed in deionized water (40 mL) and stirred for 30 min, forming a stable suspension. Simultaneously, to control the SnO_2 contents, three varying amounts of GO were added into above mixture by sonication, respectively. The resultant mixture was transferred to 50 mL Teflon-lined stainless steel autoclave, kept at 180 °C for 24 h in an oven. Afterwards, samples were washed using absolute ethyl alcohol and deionized water via centrifugation, and then freeze-dried. Three products were denoted as SnO_2/GAs-I, SnO_2/GAs-II, and SnO_2/GAs-III, respectively. As a comparison, pristine GAs were prepared via same approach without SnO_2 soliquid.

2.3. Physical characterization

The morphologies of samples were researched via scanning electron microscopy (SU8010 Hitachi/Gemini500 ZEISS; SEM) as well as transmission electron microscopy (FEI Tecnai G^2 F20; TEM). Raman spectra were performed on LabRAM HR800. Structure for prepared materials was studied by X-ray diffraction (DX-2700; XRD). The surface element states of products were researched via X-ray photoelectron spectroscopy (VG ESCALAB MK II; XPS). SnO_2 contents in nanocomposites were determined by thermogravimetric analysis (Pyris Diamond6000 TG/DTA, PerkinElmer Co, America; TGA) ranging from 25 °C to 700 °C in air.

2.4. Electrochemical characterization

To fabricate a working electrode, active materials (80 wt%), polyvinylidene fluoride (10 wt%), and conductive carbon black (10 wt%)

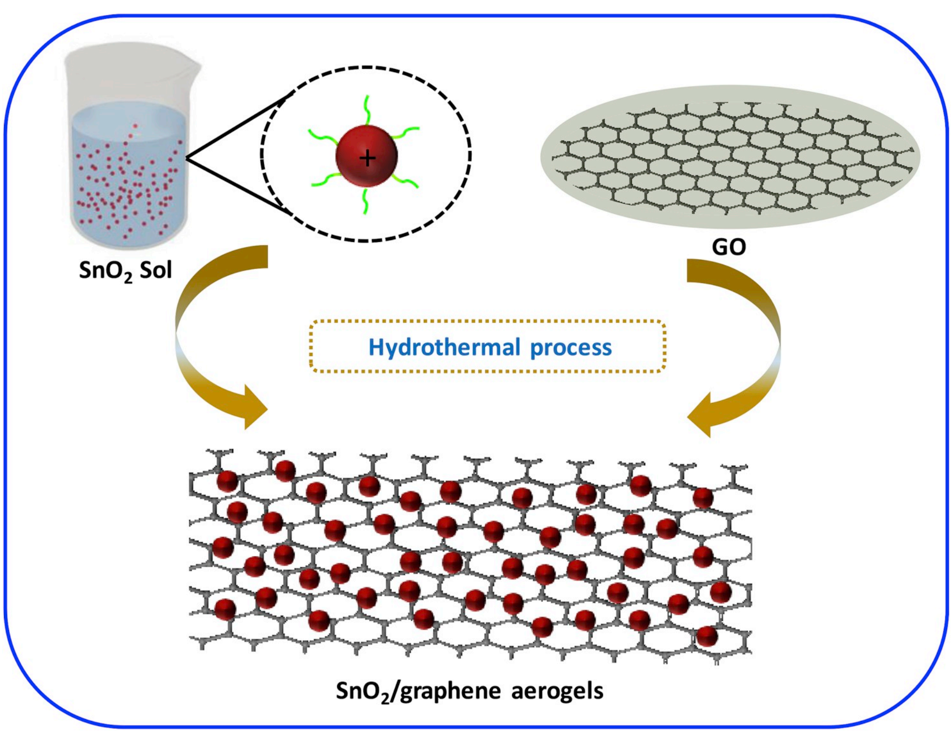

Scheme 1. Schematic illustration of the synthesis of SnO_2/graphene aerogels nanocomposites.

were added into uniform slurry in N-methyl pyrrolidone (NMP), coating on copper foil and then drying in vacuum. Afterwards, the electrodes were punched into 12 mm disks in diameter, and the mass loading of active materials was about 0.68 mg cm^{-2}. The lithium/sodium metal plates were employed as the counter and reference electrodes for LIB/SIB. 1.0 M $LiPF_6$ solution in ethylene carbonate (EC) and dimethyl carbonate (DMC) (1:1, vol/vol) was used as electrolyte of LIBs, and porous polypropylene as the separator. The electrolyte of SIBs was 1.0 M $NaClO_4$ in ethylene carbonate (EC) and propylene carbonate (PC) (2:1, vol/vol) with a 10 vol% fluoroethylene carbonate (FEC), and the glass fibre (GF/F, Whatman) as the separator. The 2032 typed coin cells were assembled in a high purity argon-filled glove box. All cells were tested using battery tester (LANHE CT2001A) between fixed voltage limits of 3.0 to 0.01 V. The cyclic voltammograms (CV) tests were performed between 0.01 and 3.0 V via Princeton Applied Research VersaSTAT4 electrochemical workstation, which was also used to test electrochemical impedance spectroscopy (EIS) with a potential amplitude of 5 mV and frequency ranging from 100 kHz to 0.01 Hz. All electrochemical characterizations were performed at room temperature.

3. Results and discussion

As observed from XRD measurement (Fig. 1a) that the diffraction peaks of SnO_2/GAs-I, SnO_2/GAs-II, and SnO_2/GAs-III located at 26.6°, 33.7°, 37.9°, 51.7°, and 65.9° correspond to (110), (101), (200), (211), and (301) crystal faces, which indicates that SnO_2 nanoparticles are formed during the hydrothermal process [17]. For pristine GAs, the diffraction peaks at $2\theta \approx 24.5°$ and 43.4° correspond with (002) and (100) planes of graphite, respectively [18]. Raman spectra measurements are carried out to prove the presence of carbon and to characterize the vibrational modes of anodes (see Fig. S1). G band puts down to vibration of sp^2 bonded carbon atoms, and D band puts down to disorder and defects in hexagonal graphitic layer [19]. I_D/I_G value is about 2.26 for pristine GAs. By comparison, it is 2.18, 2.06, and 2.00 for SnO_2/GAs-I, SnO_2/GAs-II, and SnO_2/GAs-III, respectively. The reduced I_D/I_G values suggest improved ordering of GAs layer [20,21]. Moreover, TGA is performed to evaluate SnO_2 contents in SnO_2/GAs composites (Fig. 1b). The dramatic weight loss ranging from 200 °C to 520 °C results from burning of GAs. Therefore, weight percentages of SnO_2 in SnO_2/GAs-I, SnO_2/GAs-II, and SnO_2/GAs-III are 36%, 69%, and 82%, respectively.

XPS measurements are employed to explore the elemental composition and the chemical-bonding environment of as-prepared products. Survey scan results of SnO_2/GAs-II and SnO_2/GAs-III show the existence of C, O, and Sn elements (Fig. 2a). By comparison, no obvious peaks of Sn element are found for pristine GAs. Moreover, as shown in Fig. 2b, two peaks at 494.7 and 487.6 eV represent binding energies of Sn 3d3/2 and Sn 3d5/2, indicating formation of Sn^{4+} [22]. From O 1s spectra in Fig. 2c, it can be identified that three samples show a common peak at 531.2 eV, which results from C=O groups or shoulder peak of O 1s in SnO_2. Additionally, compared with both SnO_2/GAs, the pristine GAs exhibit an extra peak (533.0 eV), corresponding to C–O–C or C–OH groups [23]. In Fig. 2d ~ f, the C 1s spectra can be resolved into four sections, which are centered at 284.2, 286.1, 287.5, 289.2 eV and assigned to C–C (sp^2 C), C–O, C=O, O–C=O groups, respectively [24]. Compared with that of pristine GAs, peak intensities of epoxide groups-C sharply decrease for SnO_2/GAs-II and SnO_2/GAs-III due to these groups possibly have bonding with SnO_2 [25].

The morphologies of products are identified by SEM. Fig. 3ã c exhibit SnO_2 nanoparticles are anchored on the two-dimensional GAs forming a sandwich-like structure and the diameter is ranged in 5–10 nm. Apparently, the loading of SnO_2 nanoparticles increases in turn, in accordance with the analytic results of TGA. Notably, for SnO_2/GAs-III, the particles aggregation phenomenon occurs severely, which may be the primary factor for the poor electrochemical property. Fig. 3d and e demonstrate TEM images of SnO_2/GAs-II, in which the 5–8 nm-sized and well-distributed SnO_2 nanoparticles could be discerned clearly. The lattice fringe d-spacings of 0.335 nm and 0.265 nm are associated with (110) and (101) interplanar distances of rutile SnO_2 [26]. In Fig. 3f, the ring-like SAED pattern is well indexed to pure phase of SnO_2, in accordance with the diffraction peaks of (110), (101), (211), (301), and (200) planes in XRD pattern, suggesting the polycrystalline nature of composites. In addition, the uniformity of SnO_2/GAs-II is also proven by the element mapping, as shown in Fig. 3g ~ j (Fig. S2 for SnO_2/GAs-I and SnO_2/GAs-III). Clearly, Sn, C, and O signals are homogeneously distributed within the chosen region, which further demonstrates the uniformly dispersion of SnO_2 nanoparticles on GAs.

Electrochemical performance of as-prepared samples for LIBs is investigated. For all SnO_2/GAs electrodes, the specific capacities are calculated in view of the full mass of the composites. Fig. 4a exhibits the first four CV curves of SnO_2/GAs-II ranging from 0.01 to 3.0 V (Figs. S3a and b for SnO_2/GAs-I and SnO_2/GAs-III). For all composites, the characteristics of these curves are assigned to reaction mechanism of SnO_2 anode during cycling, as shown by Eqs. (1) and (2):

$$SnO_2 + 4Li^+ + 4e^- \rightarrow Sn + 2Li_2O \tag{1}$$

$$Sn + xLi^+ + xe^- \leftrightarrow Li_xSn \tag{2}$$

In the initial cycle, one can see that cathodic peak at 0.81 V results from conversion of SnO_2 to Sn and generation of solid electrolyte interface (SEI) film, which is in good agreement with Eq. (1) [27]. Notably, this reduction peak shifts to 1.05 V in the following scanning cycles, which further reveals irreversibility of the reaction during the first cycle [28]. Two clear oxidation peaks (0.10 and 0.62 V) could be observed, standing for the alloying/de-alloying of Li_xSn, as described by Eq. (2), and the reversible alloying/de-alloying reactions are mainly contributive to lithium storage capacity. Another oxidation peak (1.25 V) results from the transformation from Sn to SnO or SnO_2,

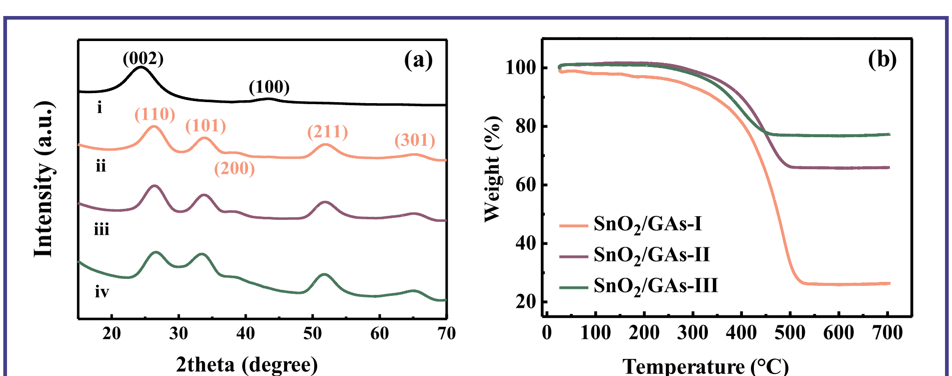

Fig. 1. (a) XRD patterns of (i) pristine GAs, (ii) SnO_2/GAs-I, (iii) SnO_2/GAs-II, and (iv) SnO_2/GAs-III; (b) TGA curves of SnO_2/GAs-I, SnO_2/GAs-II, and SnO_2/GAs-III.

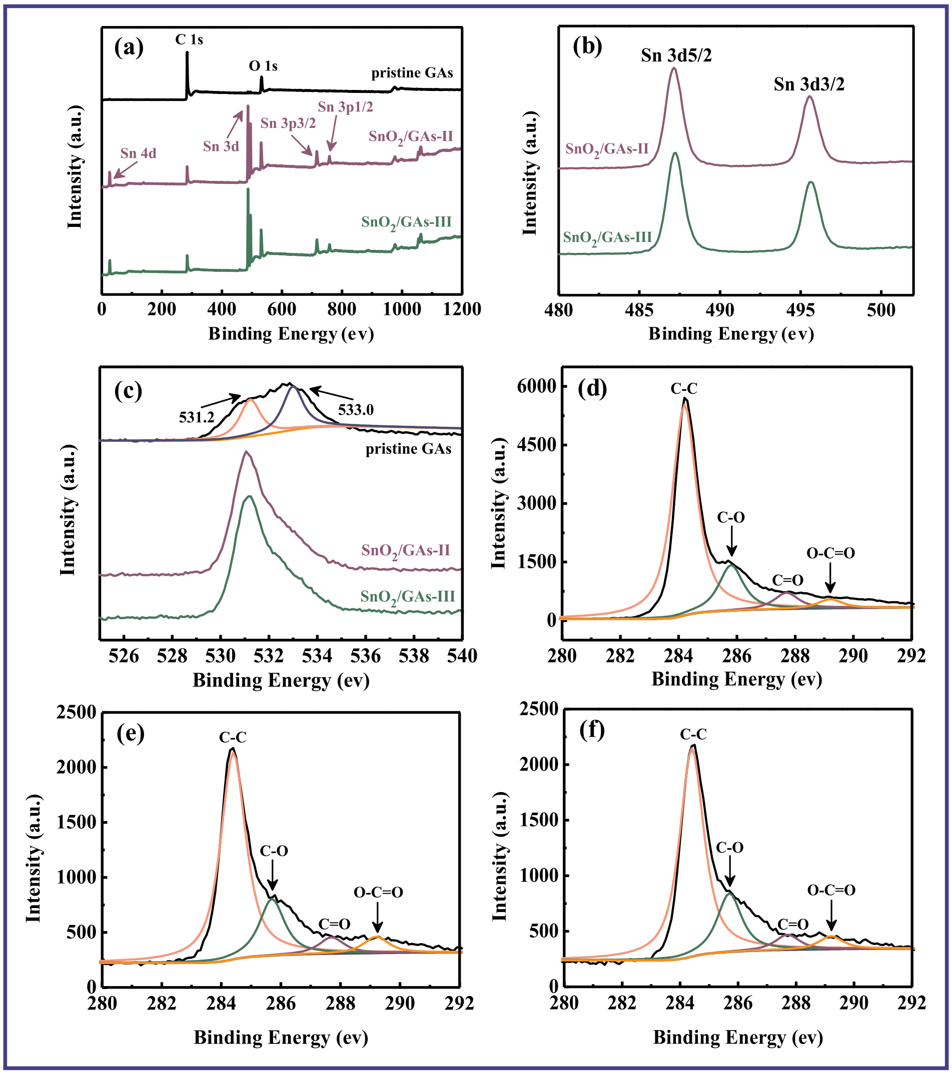

Fig. 2. (a) The survey XPS spectra of pristine GAs, SnO_2/GAs-II, and SnO_2/GAs-III; (b) Sn 3d spectra of SnO_2/GAs-II and SnO_2/GAs-III; (c) O 1s spectra of pristine GAs, SnO_2/GAs-II, and SnO_2/GAs-III; C 1s spectra of (d) pristine GAs, (e) SnO_2/GAs-II, and (f) SnO_2/GAs-III.

indicating that the partial reversibility of Eq. (1) [29,30]. Fig. 4b presents charge/discharge tests of SnO_2/GAs-II (Figs. S3c and d for SnO_2/GAs-I and SnO_2/GAs-III). In first cycle, discharge (charge) capacities of SnO_2/GAs-I, SnO_2/GAs-II, and SnO_2/GAs-III anodes are estimated to be 1004.1 (796.9), 1553.3 (960.1), and 1357.8 (745) mAh g^{-1}. Massive irreversible capacities of these electrodes probably result from decomposition of electrolyte upon lithiation as well as formation of SEI layer. In addition, compared with SnO_2/GAs-I and SnO_2/GAs-III, discharge/charge capacities of SnO_2/GAs-II are relatively consistent during cycling, suggesting that the cyclic performance tends to be stable.

As observed from Fig. 4c, cycling capacities of bare SnO_2 (see supporting materials for the detailed synthesis information) and pristine GAs are inferior and unstable at 100 mA g^{-1}. Moreover, the aggregation phenomenon of SnO_2 particles is severe (see Fig. S4), which can be responsible for the poor electrochemical performance. Theoretically, the designed SnO_2/GAs anodes are supposed to own enhanced electrochemical property due to synergistic effect. However, the cyclic performance of SnO_2/GAs-III composite is also not satisfactory. Upon 100 cycles, its reversible capacity declines rapidly to 467.6 mAh g^{-1}, the corresponding retention is approximately 55.0% (compared to the 2nd cycle, 849.4 mAh g^{-1}). The essential factors include that high SnO_2 loading leads to severe aggregation and some active materials lose electrical contact with the matrix due to volume expansion upon cycling. Whereas, with the increasing of GAs, it can ensure the uniform distribution of SnO_2 nanoparticles, along with the high surface area of GAs, the volume expansion of SnO_2 can be effectively restrained. Hence, SnO_2/GAs-I anode obtains the improved capacity of 709.6 mAh g^{-1} in the 100th cycle. However, due to the low loading of SnO_2, finite SnO_2 particles can't sufficiently exploit the high specific surface area of GAs, and the SnO_2/GAs-I contained less SnO_2 has the lower theoretical specific capacity, resulting in the cycling performance with a certain degree of limitation. Fortunately, SnO_2/GAs-II composite with suitable SnO_2 content presents the best cycling performance for all as-prepared products. It remains stable at around 818.5 mAh g^{-1} when the test is prolonged to 100 cycles. Notably, the cycling curves of as-prepared samples are not smooth due to the variable temperature in the testing room. Rate capacity under various current densities is performed to further study electrochemical property of SnO_2/GAs composites (Fig. 4d). Impressively, compared with SnO_2/GAs-I and SnO_2/GAs-III, SnO_2/GAs-II manifests exceptional rate capabilities of 853.3, 716.3, 625.5, and 542.4 mAh g^{-1} at 100, 200, 400, and 800 mA g^{-1}. Besides, reversible capacity can recover completely when current density is decreased to 100 mA g^{-1}.

The cyclability of SnO_2/GAs-II is investigated at higher current densities (Fig. 5a). It still achieves the excellent reversible capacity of 935 mAh g^{-1} upon 350 cycles under 100 mA g^{-1}, accounting for 98.8%

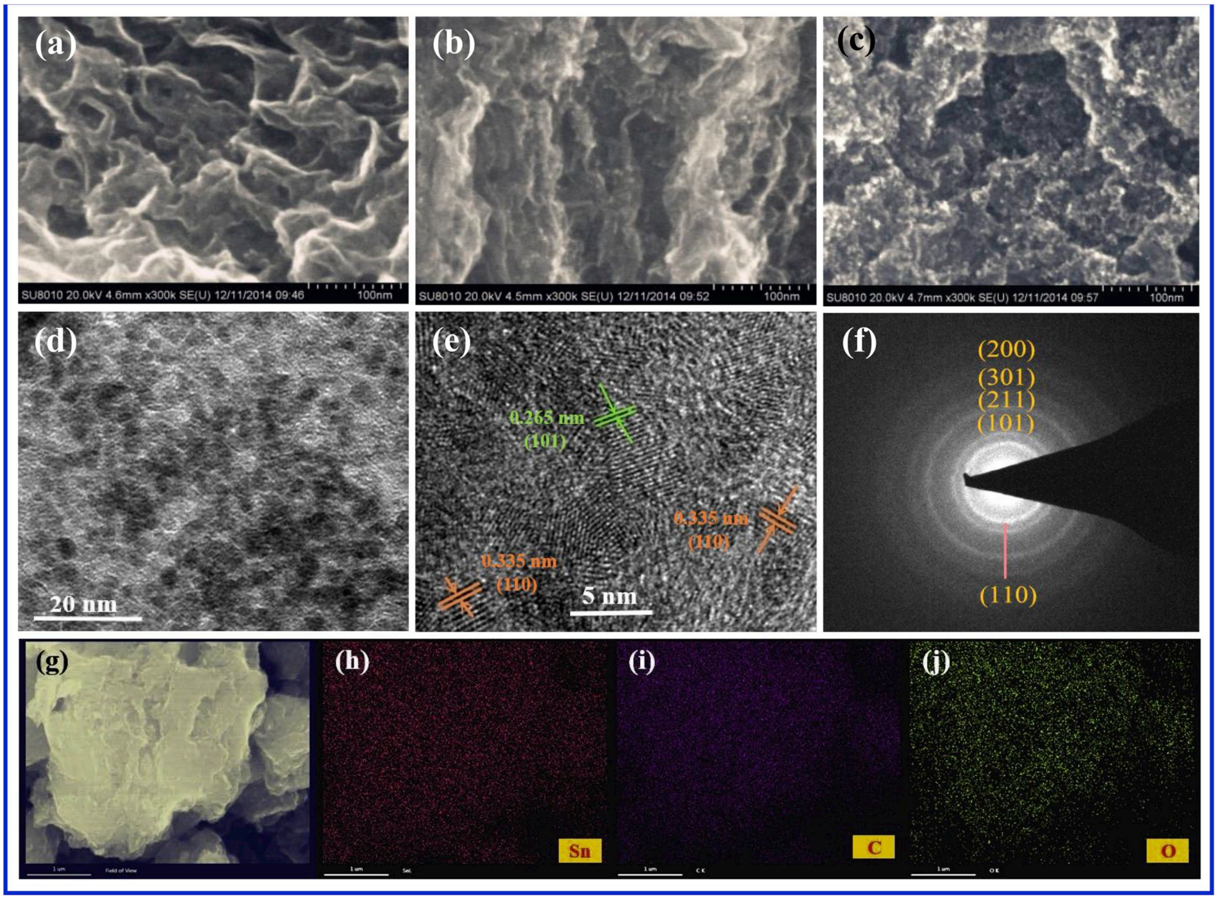

Fig. 3. Typical SEM images of (a) SnO_2/GAs-I, (b) SnO_2/GAs-II, and (c) SnO_2/GAs-III; The characteristics of SnO_2/GAs-II: (d) TEM image, (e) HRTEM image, (f) selected-area diffraction (SAED) pattern, (g ~ j) the elemental mapping images.

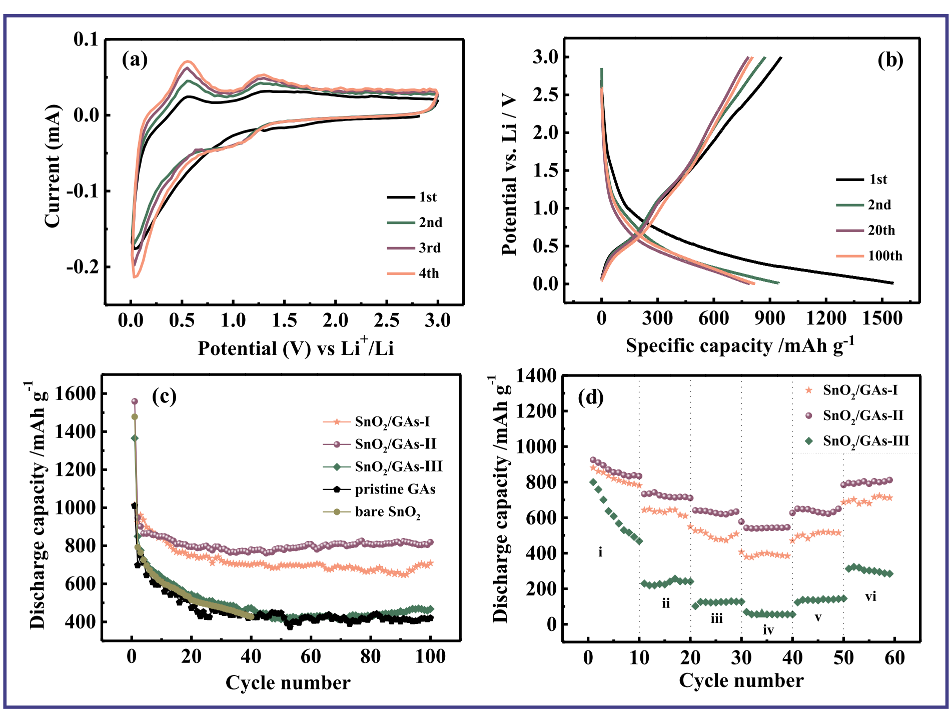

Fig. 4. Electrochemical performance for LIBs: (a) The cyclic voltammetry curves of SnO_2/GAs-II at a scan rate of 0.1 mV s^{-1} in the voltage range of 0.01–3.0 V; (b) The discharge/charge profiles of SnO_2/GAs-II in the 1st, 2nd, 20th, and 100th cycles; (c) Comparison of the cyclic performance of pristine GAs, bare SnO_2, SnO_2/GAs-I, SnO_2/GAs-II, and SnO_2/GAs-III at a current density of 100 mA g^{-1}; (d) Rate capability of SnO_2/GAs-I, SnO_2/GAs-II, and SnO_2/GAs-III at various current densities: (i) 100, (ii) 200, (iii) 400, (iv) 800, (v) 400, (vi) 100 mA g^{-1}.

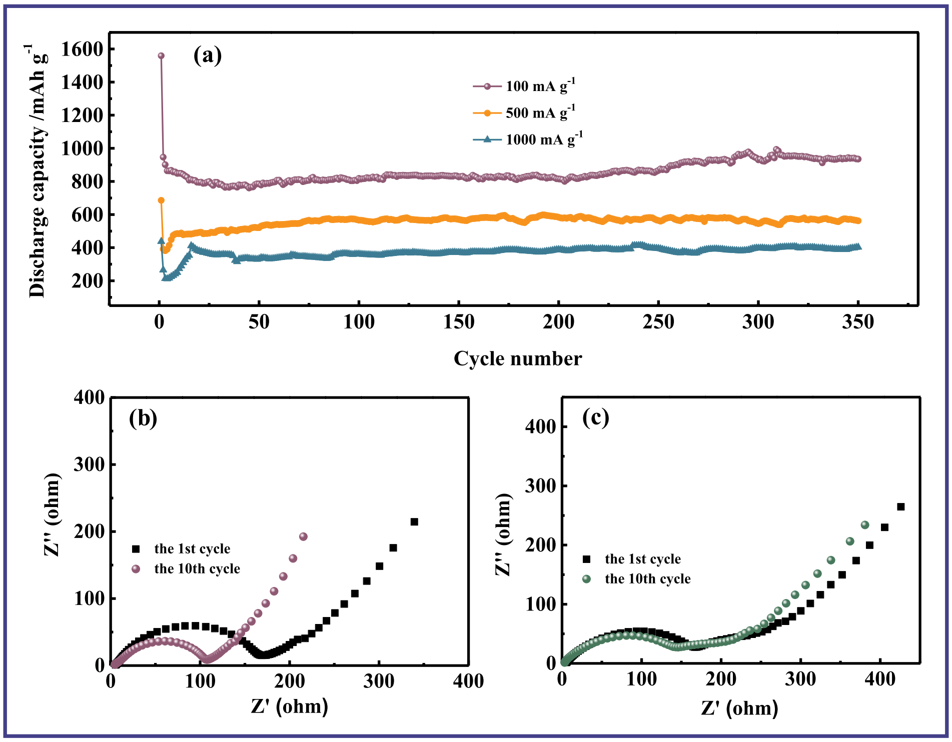

Fig. 5. Electrochemical performance for LIBs: (a) Comparison of the cyclic performance of SnO_2/GAs-II at various current densities of 100, 500, and 1000 mA g^{-1}; The electrochemical impedance spectroscopy of (b) SnO_2/GAs-II and (c) SnO_2/GAs-III in the 1st and 10th cycles at a charged state of 0.6 V.

of the 2nd reversible capacity. Meanwhile, at 500 and 1000 mA g^{-1}, capacities reach 562.4 and 402.8 mAh g^{-1} after 350 cycles (capacity retentions are 143.6% and 151.9% compared with the 2nd cycle value, respectively). Therefore, it can be speculated that SnO_2/GAs-II composite anode still possesses good reversibility even in the high current density and prolonged circle number. Compared with the SnO_2-based anode materials reported by others, the lithium storage performance of SnO_2/GAs-II is competitive and even better in terms of high capacity and long life, as shown in Table S1. EIS is carried out to investigate the mechanism for the different cycle performance of SnO_2/GAs-II and SnO_2/GAs-III composites (see Fig. 5b and c). Apparently, the charge transfer resistances (R_{ct}) are similar at first cycle for SnO_2/GAs-II (168 Ω) and SnO_2/GAs-III (172 Ω). After 10 cycles, the R_{ct} of SnO_2/GAs-II is rapidly reduced to 108 Ω, which is smaller than that of SnO_2/GAs-III (146 Ω). EIS analysis confirms that the high conductivity of SnO_2/GAs-II and thus extremely accelerates rapid electron transport during repeated lithiation-delithiation cycles [31].

SIB is also assembled to further study the outstanding electrochemical performance of as-prepared nanocomposites. The redox couple properties of SnO_2/GAs-II are presented by CV curves in Fig. 6a (Figs. S5a and b for SnO_2/GAs-I and SnO_2/GAs-III). The reaction process is represented by Eqs. (3) and (4):

$$SnO_2 + 4Na^+ + 4e^- \rightarrow Sn + 2Na_2O \tag{3}$$

$$Sn + xNa^+ + xe^- \leftrightarrow Na_xSn \tag{4}$$

During initial cathodic scan, broad irreversible peaks around 1.3 and 1.0 V are assigned to irreversible reduction of electrolyte to form SEI film and reaction for SnO_2 to Sn [32]. The peak at 1.5 V in the oxidation process corresponds to the reversible de-alloying of Na_xSn [33]. The voltammograms are superimposable after the first cycle, indicating stable oxidation/reduction reaction and high reversibility of these SnO_2/GAs anodes. Fig. 6b presents the discharge/charge profiles for SnO_2/GAs-II at 50 mA g^{-1} (Figs. S5c and d for SnO_2/GAs-I and SnO_2/GAs-III). As can be seen, a characteristic irreversible discharge plateau from 0.7 to 1.25 V is observed, which results from formation of SEI film and irreversible reaction between SnO_2 and Na^+. For SnO_2/GAs-II electrode, the initial discharge/charge capacities are 711.4/274.9 mAh g^{-1}, which are higher than that of SnO_2/GAs-I and SnO_2/GAs-III electrodes. In the subsequent cycle, SnO_2/GAs-II delivers discharge capacities of 300, 268.5, and 274 mAh g^{-1} in the 2nd, 50th, and 100th cycles, respectively, showing good electrochemical stability.

In Fig. 6c, cycle performance is conducted at 50 mA g^{-1} via galvanostatic measurements. Capacity of pristine GAs fades from 538 to 132 mAh g^{-1} upon 100 cycles. Meanwhile, the bare SnO_2 also exhibits poor cycle life. By comparison, SnO_2/GAs with different mass loading shows enhanced electrochemical performance. As expected, SnO_2/GAs-II achieves a superior reversible capacity of 274 mAh g^{-1} in the 100th cycle. However, SnO_2/GAs-I and SnO_2/GAs-III deliver lower reversible capacities of 207 and 190 mAh g^{-1}. More strikingly, for SnO_2/GAs-II electrode, the retentive capacity of 274 mAh g^{-1} up to 100 cycles is 91.3% of the second cycle capacity (300 mAh g^{-1}), showing outstanding electrochemical stability. While capacity retentions of SnO_2/GAs-I and SnO_2/GAs-III are 71.9% and 76.4%, respectively. Moreover, as shown in Fig. 6d, SnO_2/GAs-II also shows a better rate capability at various current densities than that of SnO_2/GAs-I and SnO_2/GAs-III. The retained discharge capacities of three SnO_2/GAs anodes at 50, 100, 200, and 400 mA g^{-1} are compared, as described in Fig. S6, the SnO_2/GAs-II is observed to sustain high capacity retention. Fig. 6e and f display the impedance spectra of SnO_2/GAs-II and SnO_2/GAs-III samples (Figs. S7a and b for pristine GAs and SnO_2/GAs-I). As a whole, the R_{ct} of all electrodes decrease with the increase of discharge depth (Table S2), illustrating that sodium insertion gradually enhances electronic conductivity of electrodes. In addition, R_{ct} for SnO_2/GAs-II electrode is smaller than those of other electrodes in the 1st and 5th cycles, respectively, suggesting that SnO_2/GAs-II electrode possesses an enhanced electron and sodium ion transport.

Based on the above discussion, SnO_2/GAs-II shows obvious advantages as anode material in LIBs and SIBs, which are attributed to the following points: (1) the synthesized SnO_2 soliquid has high stability and

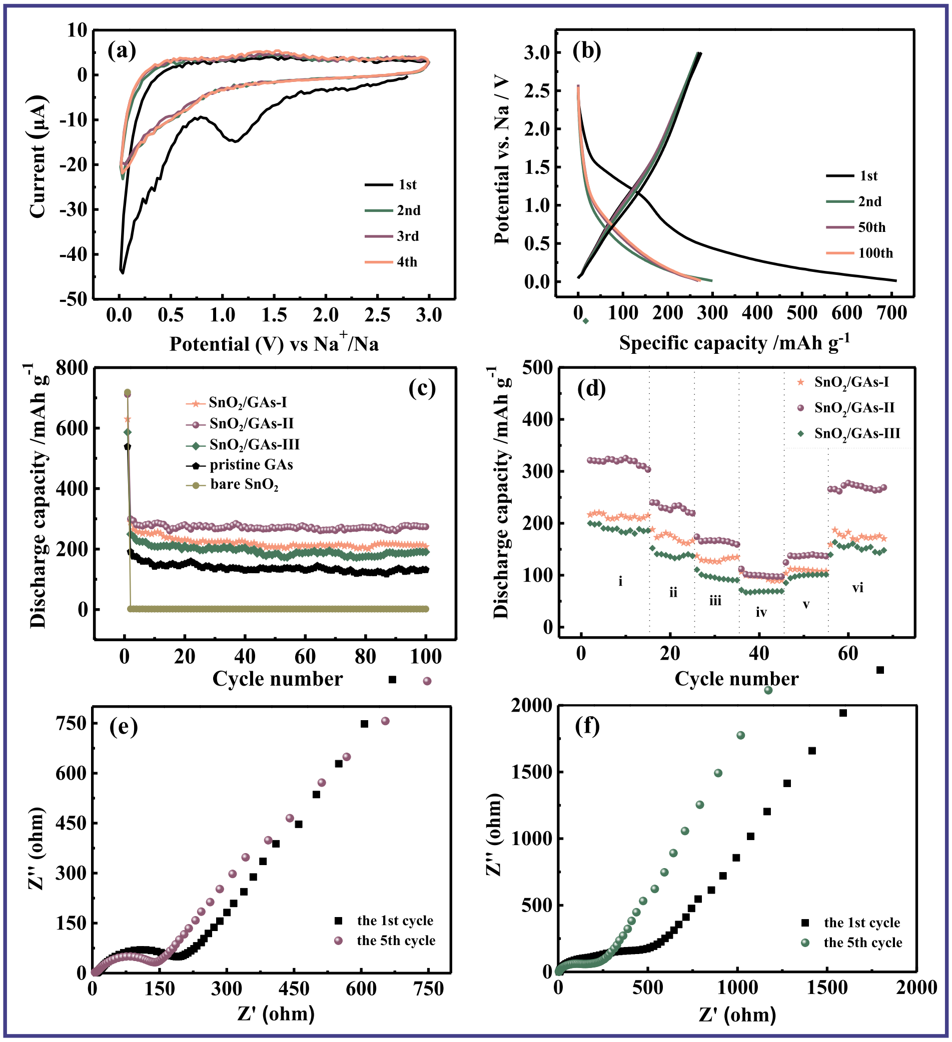

Fig. 6. Electrochemical performance for SIBs: (a) The cyclic voltammetry curves of SnO_2/GAs-II at a scan rate of 0.1 mV s^{-1} in the voltage range of 0.01–3.0 V; (b) The discharge/charge profiles of SnO_2/GAs-II in the 1st, 2nd, 50th, and 100th cycles; (c) Comparison of the cyclic performance of pristine GAs, bare SnO_2, SnO_2/GAs-I, SnO_2/GAs-II, and SnO_2/GAs-III at a current density of 50 mA g^{-1}; (d) Rate capability of SnO_2/GAs-I, SnO_2/GAs-II, and SnO_2/GAs-III at various current densities: (i) 50, (ii) 100, (iii) 200, (iv) 400, (v) 200, (vi) 50 mA g^{-1}; The electrochemical impedance spectroscopy of (e) SnO_2/GAs-II and (f) SnO_2/GAs-III in the 1st and 5th cycles at a charged state of 1.5 V.

reactivity, and the electrostatic interaction between positively charged SnO_2 soliquid and negatively charged GAs ensures the structural integrity of composites; (2) the suitable SnO_2 contents in composites can guarantee the uniform distribution of nanoparticles and make full use of the GAs matrix, revealing a most effective combination advantages of composites; (3) the small size of SnO_2 nanoparticles can maintain high contact area with electrolyte, decrease diffusion lengths, and enhance lithium/sodium diffusion kinetics [34]; (4) high surface area of GAs can effectively relieve SnO_2 expansion/shrinkage upon cycling.

In order to further investigate the structure stability of SnO_2/GAs-II electrode in LIBs and SIBs, SEM images of SnO_2/GAs-II electrodes after 100 charge/discharge cycles are collected and shown in Figs. S8a and b. As anode material of LIBs, the initial morphology of the SnO_2/GAs-II has been well maintained at the end of the 100 cycles. The volumetric expansion during the repeated cycles has been restricted due to the GAs sheets. However, as anode material of SIBs, the structural integrity of SnO_2/GAs-II is destroyed after the long-term cycles. Because of the large radius of Na^+, the resultant SnO_2 suffers from more severe volume expansion upon alloying with Na, which can make the SnO_2 active material become vulnerable [35]. The structural integrity of the electrode materials is the precondition for the cyclic stability, hence the cyclic performance of SnO_2/GAs in LIBs is superior than that of SIBs.

4. Conclusions

In summary, this work systemically investigates the effect of different SnO_2 contents in nanocomposites for both anodes of LIBs and SIBs. An appropriate amount of SnO_2 nanoparticles in composites can sufficiently exploit the high specific surface area of GAs, as a result, particles aggregation phenomenon can be avoided so as to mitigate the enormous volume expansion during charge-discharge processes. Furthermore, due to the SnO_2 soliquid as the precursor, the resultant SnO_2 nanoparticles with the diameter of 5–8 nm show high stability and reactivity. More importantly, the electrostatic interaction between SnO_2 soliquid and GAs guarantees the structural integrity of anode materials. Surprisingly, as anode material for LIBs, the optimized SnO_2/GAs nanocomposite with suitable SnO_2 loading presents the superior reversible capacity of 935 mAh g^{-1} at 100 mA g^{-1} upon 350 cycles. Meanwhile, it still shows excellent rate capacities of 562.4 and 402.8 mAh g^{-1} even under high current densities of 500 and 1000 mA g^{-1}. As anode material for SIBs, SnO_2/GAs exhibits long-term cyclic stability and excellent electrical conductivity. It maintains the capacity of 274 mAh g^{-1} in the 100th cycle under 50 mA g^{-1}, according with 91.3% of the 2nd reversible capacity. Therefore, we believe this study may open a new ideal for designing SnO_2-based anode materials with excellent cyclic performance.

Acknowledgements

This research was supported by the National Key Research and Development Program of China (2018YFB0105900).

Appendix A. Supplementary data

Supplementary data to this article can be found online at https://doi.org/10.1016/j.matchemphys.2019.121870.

References

[1] Y. Li, J. Liu, Y. Lei, C. Lai, Q. Xu, Enhanced electrochemical performances of Na-doped cathode material $LiNi_{1/3}Co_{1/3}Mn_{1/3}O_2$ for lithium-ion batteries, J. Mater. Sci. 52 (2017) 13596–13605.

[2] C. Chen, Y. Wen, X. Hu, X. Ji, M. Yan, L. Mai, P. Hu, B. Shan, Y. Huang, Na(+) intercalation pseudocapacitance in graphene-coupled titanium oxide enabling ultra-fast sodium storage and long-term cycling, Nat. Commun. 6 (2015) 6929.

[3] S. Komaba, W. Murata, T. Ishikawa, N. Yabuuchi, T. Ozeki, T. Nakayama, A. Ogata, K. Gotoh, K. Fujiwara, Electrochemical Na insertion and solid electrolyte interphase for hard-carbon electrodes and application to Na-ion batteries, Adv. Funct. Mater. 21 (2011) 3859–3867.

[4] J.B. Goodenough, Rechargeable batteries: challenges old and new, J. Solid State Electrochem. 16 (2012) 2019–2029.

[5] Y. Yue, H. Liang, Micro- and nano- structured vanadium pentoxide (V_2O_5) for electrodes of lithium-ion batteries, Adv. Energy Mater. 7 (2017) 1602545.

[6] D. Luo, J. Xu, Q.B. Guo, L.Z. Fang, X.H. Zhu, Q.Y. Xia, H. Xia, Surface-dominated sodium storage towards high capacity and ultrastable anode material for sodium-ion batteries, Adv. Funct. Mater. 28 (2018) 1805371.

[7] J.D. Xie, H.Y. Li, B. Umesh, T.C. Lee, J.K. Chang, Y.A. Gandomi, Prior vacuuming for supercritical fluid synthesis of SnO_2/graphene nanocomposites with superior electrochemical Li^+ storage performance, Electrochim. Acta 292 (2018) 951–959.

[8] X. Zhao, M. Luo, W.X. Zhao, R.M. Xu, Y. Liu, H. Shen, SnO_2 nanosheets anchored on a 3D, bicontinuous electron and ion transport carbon network for high-performance sodium-ion batteries, ACS Appl. Mater. Interfaces 10 (2018) 38006–38014.

[9] L. Zhang, K. Zhao, W. Xu, Y. Dong, R. Xia, F. Liu, L. He, Q. Wei, M. Yan, L. Mai, Integrated SnO_2 nanorod array with polypyrrole coverage for high-rate and long-life lithium batteries, Phys. Chem. Chem. Phys. 17 (2015) 7619–7623.

[10] Y. Wang, Y. Jin, C. Zhao, Y. Duan, X. He, M. Jia, SnO_2 quantum dots/graphene aerogel composite as high-performance anode material for sodium ion batteries, Mater. Lett. 191 (2017) 169–172.

[11] P. Dou, Z.Z. Cao, C. Wang, J. Zheng, X.H. Xu, Multilayer Zn-doped SnO_2 hollow nanospheres encapsulated in covalently interconnected three-dimensional graphene foams for high performance lithium-ion batteries, Chem. Eng. J. 320 (2017) 405–415.

[12] V. Sridhar, H. Park, Hollow SnO_2@ carbon core-shell spheres stabilized on reduced graphene oxide for high-performance sodium-ion batteries, New J. Chem. 41 (2017) 442–446.

[13] X. Li, X. Li, L. Fan, Z. Yu, B. Yan, D. Xiong, X. Song, S. Li, K.R. Adair, D. Li, X. Sun, Rational design of Sn/SnO_2/porous carbon nanocomposites as anode materials for sodium-ion batteries, Appl. Surf. Sci. 412 (2017) 170–176.

[14] D.A. Zhou, X.G. Li, L.Z. Fan, Y.H. Deng, Three-dimensional porous graphene-encapsulated CNT@SnO_2 composite for high-performance lithium and sodium storage, Electrochim. Acta 230 (2017) 212–221.

[15] X. Li, Y. Hu, J. Liu, A. Lushington, R. Li, X. Sun, Structurally tailored graphene nanosheets as lithium ion battery anodes: an insight to yield exceptionally high lithium storage performance, Nanoscale 5 (2013) 12607–12615.

[16] X. Li, X. Meng, J. Liu, D. Geng, Y. Zhang, M.N. Banis, Y. Li, J. Yang, R. Li, X. Sun, M. Cai, M.W. Verbrugge, Tin oxide with controlled morphology and crystallinity by atomic layer deposition onto graphene nanosheets for enhanced lithium storage, Adv. Funct. Mater. 22 (2012) 1647–1654.

[17] B. Huang, Z. Pan, X. Su, L. An, Tin-based materials as versatile anodes for alkali (earth)-ion batteries, J. Power. Sources 395 (2018) 41–59.

[18] Z.J. Zhang, Y.X. Wang, S.L. Chou, H.J. Li, H.K. Liu, J.Z. Wang, Rapid synthesis of α-Fe_2O_3/rGO nanocomposites by microwave autoclave as superior anodes for sodium-ion batteries, J. Power. Sources 280 (2015) 107–113.

[19] Y.G. Zhu, Y. Wang, J. Xie, G.S. Cao, T.J. Zhu, X. Zhao, H.Y. Yang, Effects of graphene oxide function groups on SnO_2/graphene nanocomposites for lithium storage application, Electrochim. Acta 154 (2015) 338–344.

[20] Z. Wu, X. Li, L. Tai, H. Song, Y. Zhang, B. Yan, L. Fan, H. Shan, D. Li, Novel synthesis of tin oxide/graphene aerogel nanocomposites as anode materials for lithium ion batteries, J. Alloy. Comp. 646 (2015) 1009–1014.

[21] H. Song, N. Li, H. Cui, C. Wang, Enhanced capability and cyclability of SnO_2-graphene oxide hybrid anode by firmly anchored SnO_2 quantum dots, J. Mater. Chem. A 1 (2013) 7558–7562.

[22] Y. He, A. Li, C. Dong, C. Li, L. Xu, Mesoporous tin-based oxide nanospheres/reduced graphene composites as advanced anodes for lithium-ion half/full cells and sodium-ion batteries, Chem. Eur J. 23 (2017) 13724–13733.

[23] W. Lv, D.M. Tang, Y.B. He, C.H. You, Z.Q. Shi, X.C. Chen, C.M. Chen, P.X. Hou, C. Liu, Q.H. Yang, Low-temperature exfoliated graphenes: vacuum-promoted exfoliation and electrochemical energy storage, ACS Nano 3 (2009) 3730–3736.

[24] L. Fan, X. Li, Y. Cui, H. Xu, X. Zhang, D. Xiong, B. Yan, Y. Wang, D. Li, Tin oxide/graphene aerogel nanocomposites building superior rate capability for lithium ion batteries, Electrochim. Acta 176 (2015) 610–619.

[25] D. Yang, A. Velamakanni, G. Bozoklu, S. Park, M. Stoller, R.D. Piner, S. Stankovich, I. Jung, D.A. Field, C.A. Ventrice Jr., R.S. Ruoff, Chemical analysis of graphene oxide films after heat and chemical treatments by X-ray photoelectron and Micro-Raman spectroscopy, Carbon 47 (2009) 145–152.

[26] D.T. Ma, Y.L. Li, H.W. Mi, S. Luo, P.X. Zhang, Z.Q. Lin, J.Q. Li, H. Zhang, Robust SnO_{2-x} nanoparticle-impregnated carbon nanofibers with outstanding electrochemical performance for advanced sodium-ion batteries, Angew. Chem. Int. Ed. 57 (2018) 8901–8905.

[27] Y.T. Xu, Y. Guo, C. Li, X.Y. Zhou, M.C. Tucker, X.Z. Fu, R. Sun, C.P. Wong, Graphene oxide nano-sheets wrapped Cu_2O microspheres as improved performance anode materials for lithium ion batteries, Nano Energy 11 (2015) 38–47.

[28] J. Chen, K. Yano, Highly monodispersed tin oxide/mesoporous starbust carbon composite as high-performance Li-ion battery anode, ACS Appl. Mater. Interfaces 5 (2013) 7682–7687.

[29] L. Zhang, M. Yang, S. Zhang, Z. Wu, A. Amini, Y. Zhang, D. Wang, S. Bao, Z. Lu, N. Wang, C. Cheng, V_2O_5-C-SnO_2 hybrid nanobelts as high performance anodes for lithium-ion batteries, Sci. Rep. 6 (2016) 33597.

[30] S.L. Yang, B.H. Zhou, M. Lei, L.P. Huang, J. Pan, W. Wu, H.B. Zhang, Sub-100nm hollow SnO_2@C nanoparticles as anode material for lithium ion batteries and significantly enhanced cycle performances, Chin. Chem. Lett. 26 (2015) 1293–1297.

[31] J.Y. Cheong, C. Kim, J.W. Jung, T.G. Yun, D.Y. Youn, S.H. Cho, K.R. Yoon, H. Y. Jang, S.W. Song, I.D. Kim, Incorporation of amorphous TiO_2 into one-dimensional SnO_2 nanostructures as superior anodes for lithium-ion batteries, J. Power Sources 400 (2018) 485–492.

[32] Y.X. Wang, Y.G. Lim, M.S. Park, S.L. Chou, J.H. Kim, H.K. Liu, S.X. Dou, Y.J. Kim, Ultrafine SnO_2 nanoparticle loading onto reduced graphene oxide as anodes for sodium-ion batteries with superior rate and cycling performances, J. Mater. Chem. A 2 (2014) 529–534.

[33] X. Li, X.H. Sun, Z.W. Gao, X.D. Hu, R. Ling, S. Cai, C.M. Zheng, W.B. Hu, Highly reversible and fast sodium storage boosted by improved interfacial and surface charge transfer derived from the synergistic effect of heterostructures and pseudocapacitance in SnO_2-based anodes, Nanoscale 10 (2018) 2301–2309.

[34] H. Wang, Y.M. Wu, Y.S. Bai, W. Zhou, Y.R. An, J.H. Li, L. Guo, The self-assembly of porous microspheres of tin dioxide octahedral nanoparticles for high performance lithium ion battery anode materials, J. Mater. Chem. 21 (2011) 10189–10194.

[35] H.G. Wang, C. Jiang, C.P. Yuan, Q. Wu, Q. Li, Q. Duan, Complexing agent engineered strategy for anchoring SnO_2 nanoparticles on sulfur/nitrogen co-doped graphene for superior lithium and sodium ion storage, Chem. Eng. J. 332 (2018) 237–244.